Comprehensive Demonstration of Spin Hall Hanle Effects in Epitaxial Pt Thin Films

Jing Li[1*], Andrew H. Comstock[2*], Dali Sun[2⊥], and Xiaoshan Xu[1⊥]

[1]Department of Physics and Astronomy and Nebraska Center for Materials and Nanoscience, University of Nebraska, Lincoln, NE 68588, USA

[2]Department of Physics and Organic and Carbon Electronics Lab (ORaCEL), North Carolina State University, Raleigh, NC 27695, USA

* Authors with equal contributions

⊥ xiaoshan.xu@unl.edu, dsun4@ncsu.edu

Abstract

We demonstrate a nonlinear Hall effect due to the boundary spin accumulation in Pt films grown on Al_2O_3 substrates. This Hall effect and the previously demonstrated Hanle magnetoresistance provide a complete picture of the spin-precession control of the spin and charge transport at the boundary of a spin-orbit coupled material, which we refer to as spin-Hall Hanle effects (SHHE). We also show that the SHHE can be employed to measure the spin diffusion length, the spin-Hall angle, and the spin relaxation time of heavy metal without the need of magnetic interface or the input from other measurements. The comprehensive demonstration of SHHE in such a simple system suggests they may be ubiquitous and needs to be considered for unravelling the spin and charge transport in more complex thin film structures of spin-orbit coupled materials.

Ever since the discovery of the spin Hall effect (SHE) and the inverse spin Hall effect (ISHE) [1–5], the strong spin-orbit coupling in materials such as heavy metals has been widely used for both the generation [6] and detection of pure spin current [7]. Recently, the interaction between spin current (from the SHE) in a heavy metal and the local spins in an adjacent magnetic material has been demonstrated to give rise to the spin-Hall magnetoresistance (SMR) [8,9]. This interfacial mechanism was later employed to effectively detect [10–12] and even manipulate [13] the antiferromagnetic order which is beyond the capability of bulk magnetometry.

On the other hand, it is difficult to probe SHE and ISHE as bulk effects in heavy metals using magneto-transport, because the modulation by a magnetic field is limited by the short timescale of momentum relaxation [14]. In contrast, at the boundary of the heavy metals, the spin accumulation and diffusion (spin-current reflection) may be more effectively manipulated by a magnetic field via spin precession according to the Hanle effect [Fig. 1(a)], because it is the spin relaxation that determines the timescale of the process. Given the relationship between spin diffusion and charge current as described by the ISHE, Dyakonov predicted a longitudinal effect [15], which was later observed in Pt and β-phase Ta thin films [16,17] and named Hanle magnetoresistance; one key evidence is the anisotropy since spin precession depends on the angle between the magnetic field and the initial spin polarization [16].

What's puzzling is the transverse effect. In principle, spin precession is expected to rotate the spin polarization and generate a transverse charge current corresponding to a Hall effect. However, this Hall effect has not been experimentally demonstrated and often overlooked. In particular, in the previous work [16] where the longitudinal effect was demonstrated, only a linear field-dependence of the transverse signal was observed and attributed to the ordinary Hall effect (OHE).

To resolve the puzzle of missing transverse effect, we note that the previous work [16] may have only probed the weak-precession condition due to the short spin relaxation time τ_s. In the weak-precession condition, a linear field dependence of the Hall effect is expected, which cannot be distinguished from the linear OHE background; meanwhile a quadratic field dependence of the magnetoresistance is expected which is consistent with the observation [16].

In this work, we perform a magneto-transport study on the interplay of SHE, ISHE, spin diffusion, and spin relaxation in Pt thin films deposited epitaxially on Al_2O_3 substrates using pulsed laser deposition to enhance τ_s for reaching the strong-precession condition. We observed non-quadratic and non-linear field dependence for the longitudinal (magnetoresistance) and the transverse (Hall) effects respectively, indicating the strong precession condition. The dual effects, which we refer to as the spin-Hall Hanle effects (SHHE), can be fit using the same set of parameters (spin Hall angle θ_{SH}, spin diffusion length λ_s, spin relaxation time τ_s), suggesting that SHHE can be reliably employed in extracting the spin transport properties without complications from the magnetic interfaces, such as spin memory loss [18] and proximity-induced magnetism [19,20].

Pt (111) thin films of various thickness were epitaxially grown on Al_2O_3 (0001) substrates by pulsed laser deposition with a YAG laser (266 nm wavelength, 70 mJ pulse energy, 3 Hz repetition rate) in 10^{-7} torr vacuum at room temperature and subsequently patterned into Hall bars by photolithography and ion milling. Crystal orientation of the Pt (111) films was confirmed using X-ray diffraction (Sec. S1 within the Supplemental Material [21]) while the film thickness was measured using X-ray reflectivity. Longitudinal and transverse resistivity was measured using the Hall bar (Sec. S2 within the Supplemental Material [21]) in magnetic field along different

directions at room temperature; the field dependence of the longitudinal (ρ_L) and transverse (ρ_T) resistivity was symmetrized and antisymmetrized respectively to minimize the spurious effects from imperfect device geometry.

Figure 1(b) shows the change of longitudinal resistivity $\Delta\rho_L=\rho_L-\rho_{L0}$ normalized with respect to the zero-field value ρ_{L0} in a 5.2-nm-thick Pt film, where B_x, B_y and B_z represent the magnetic field applied along the x, y, and z direction respectively. Overall, $\Delta\rho_L$ increases with the magnetic field, consistent with the expectation from the SHHE [15]. As illustrated in Fig. 1(a), the longitudinal charge current ($\vec{J}_c \parallel +\hat{x}$) in the Pt film generates a spin current ($\vec{J}_s \parallel -\hat{z}$) via SHE toward the Pt/$Al_2O_3$ interface with spin polarization $\vec{s} \parallel -\hat{y}$. The reflected spin current ($\vec{J}_{S,R} \parallel +\hat{z}$) generates a longitudinal charge current $\vec{J}_{C,R} \propto \vec{J}_{S,R} \times \vec{s} \parallel +\hat{x}$ via the ISHE before the spin polarization relaxes, resulting in an overall reduction in the resistivity of the Pt film. The Hanle effect may be observed when an external magnetic field causes the precession of the spin polarization of $\vec{J}_{S,R}$. In this case, the projection of $\vec{J}_{C,R}$ on $+\hat{x}$ will be reduced, which increases the longitudinal resistivity, as observed in Fig. 1(b) consistent with that in previous work [16].

The anisotropy in Fig. 1(b) also agrees with SHHE in that $\Delta\rho_L(B_y)/\rho_{L0}$ is smaller than $\Delta\rho_L(B_x)/\rho_{L0}$ and $\Delta\rho_L(B_z)/\rho_{L0}$ while the latter two are similar. When the magnetic field is parallel to the initial polarization direction ($\hat{y}$) of $\vec{J}_{s,R}$, no spin precession is caused by the external magnetic field and the SHHE does not contribute to $\Delta\rho_L(B_y)/\rho_{L0}$. As a result, ordinary magnetoresistance (OMR) is responsible for the non-zero $\Delta\rho_L(B_y)/\rho_{L0}$ observed in Fig. 1(b) which is proportional to B^2; hence the difference $\Delta\rho_L(B_z)$-$\Delta\rho_L(B_y)$ is attributed to the longitudinal SHHE.

Fig. 1(b) also reveals the strong-precession behavior of the longitudinal SHHE that was not observed before. Considering both the film-substrate and the film-vacuum boundaries, SHHE with B_z can be described using [15] (Sec. S3 within the Supplemental Material [21]):

$$\frac{\Delta\rho_{SHHE}}{\rho_{L0}} = \theta_{SH}^2 \frac{\tanh(d/2\lambda_s)}{d/2\lambda_s}\left[1 - \frac{\tanh\left(\frac{\kappa d}{2\lambda_s}\right)}{\kappa\cdot\tanh\left(\frac{d}{2\lambda_s}\right)}\right] \quad (1),$$

where the real and imaginary parts of $\Delta\rho_{SHHE}$ are the longitudinal $\Delta\rho_{L,SHHE}$ and the transverse $\rho_{T,SHHE}$ respectively, d is the film thickness, $\kappa = (1 - i\Omega\tau_s)^{1/2}$ is a complex quantity with $i=\sqrt{-1}$, $\Omega = g\mu_B B_z/\hbar$ is the Larmor frequency with g the gyromagnetic factor, μ_B the Bohr magneton, and $\hbar$ the reduced Planck constant. A numeric simulation is displayed in Fig. 2. According to Eq. (1) and Fig. 2(a), at low field (weak precession), the longitudinal SHHE is quadratic ($\propto B_z^2$) as observed previously [16]; at high field (strong precession), the effect saturates when the precession angle is so large that the projection of $\vec{J}_{cR}$ on $\hat{x}$ cancels, consistent with the reduced slope $\Delta\rho_L(B_x)/\rho_{L0}$ and $\Delta\rho_L(B_z)/\rho_{L0}$ at high field in Fig. 1(b).

Figure 1(c) shows the normalized transverse resistivity ρ_T/ρ_{L0}, which has non-trivial field dependence only in B_z. In addition, $\rho_T(B_z)/\rho_{L0}$ exhibits a non-linear relation with a large slope at low field and a smaller slope at high field. The latter is expected to come from the ordinary Hall effect (OHE) in a non-magnetic metal. Similar field dependence of the transverse resistivity has been observed in Pt/ferrimagnetic insulator (FMI) systems, which was explained as anomalous Hall effect caused by magnetic proximity [19,22,23]. Here we don't have the complications from the magnetic order of the substrate, so the non-linear part of the transverse signal can be directly ascribed to SHHE as explained in the following.

As illustrated in Fig. 1(a), with B_z, the spin precession leads to non-zero projection of the spin polarization of $\vec{J}_{S,R}$ on $\hat{x}$, which generates a non-zero projection of $\vec{J}_{C,R}$ on $\hat{y}$ (Hall signal) via ISHE. At low field (weak precession), the effect is linear ($\propto B_z$) according to Eq. (1) and Fig. 2(b). At high field (strong precession), the transverse effect is expected to vanish because the projection of $\vec{J}_{C,R}$ on $\hat{y}$ cancels due to the large precession angle. This overall nonlinear effect is consistent with the observation in Fig. 1(c).

The observation of the non-quadratic longitudinal and the non-linear transverse field dependence in Figs. 1(b) and (c) respectively, suggests the strong-precession condition of SHHE in Eq. (1). In principle, all the parameters contributing to SHHE, i.e., τ_s, θ_{SH}, and λ_s can be extracted by fitting the experimental data using the field dependence in Eq. (1). On the other hand, a scaling rule pointed out by Dyakonov [15] (Sec. S3 within the Supplemental Material [21]) also needs to be considered, as described below.

Considering the spin-precession nature, the SHHEs are expected to scale with the spin precession time τ_S^*. For $d/\lambda_s \to \infty$ (thick film limit), τ_S^* is limited by the spin relaxation time τ_s, i.e., $\tau_S^*=\tau_s$, as illustrated in Fig. 1(a). For $d/\lambda_s \to 0$ (thin film limit), spin precession occurs over the entire film thickness, so τ_S^* is the same as the spin diffusion time $\tau_D = \frac{\left(\frac{d}{2}\right)^2}{D} = \tau_s\left(\frac{d}{2\lambda_s}\right)^2$, where $D = \frac{\lambda_s^2}{\tau_s}$ is the spin diffusion coefficient. Dyakonov then introduced the definition $\frac{1}{\tau_S^*} = \frac{1}{\tau_s} + \frac{1}{\tau_D} = \frac{1}{\tau_s}\left[1 + \left(\frac{2\lambda_s}{d}\right)^2\right]$ to describe the dependence of τ_S^* on both τ_s and d [15]. As shown in Fig. 2, $\Delta\rho_{L,SHHE}$ and $\rho_{T,SHHE}$ simulated according to Eq. (1) are normalized with the maximum longitudinal effect $\Delta\rho_{L,SHHE}(B_z=\infty)$ and plotted as a function of $\Omega\tau_S^*$. Indeed, the "scaled" field dependence of SHHE maintains roughly the same curve shape despite that the value of d/λ_s changes over four orders of magnitude.

The Dyakonov's scaling rule suggests that it is difficult to unambiguously determine τ_s, θ_{SH}, and λ_s altogether by fitting the measured field dependence of $\Delta\rho_{SHHE}/\rho_{L0}$ using Eq. (1) considering the experimental uncertainty, because it is τ_S^* instead of τ_s that can be directly extracted. On the other hand, here we notice that λ_s can be estimated based on the thickness dependence of SHHE, which can then be used to extract τ_s (out of τ_S^*) and θ_{SH}. A close look at Eq. (1) reveals that the *low-field* $\Delta\rho_{SHHE}/\rho_{L0}$ has a maximum at an intermediate film thickness because it vanishes in both the thin and thick film limits: For $d/\lambda_s \to 0$ (thin film limit), $\Delta\rho_{SHHE}$ approaches zero because $\tau_S^* \to 0$ means no precession; for $d/\lambda_s \to \infty$ (thick limit), $\Delta\rho_{SHHE}/\rho_{L0}$ also approaches zero because the effect of the spin precession that occurs at the boundary is unimportant for thick films. It turns out that the thickness for reaching maximum *low-field* $\Delta\rho_{SHHE}/\rho_{L0}$ only depends on λ_s, or $d/\lambda_s \approx 4.56$ and $d/\lambda_s \approx 3.28$ for $\Delta\rho_{L,SHHE}/\rho_{L0}$ and $\rho_{T,SHHE}/\rho_{L0}$ respectively (Sec. S3 within the Supplemental Material [21]), as also given by Eq. S36 and Eq. S38 in ref. [16].

Considering this property, we measured the thickness dependence of SHHE in the epitaxial Pt films. The experimental $\Delta\rho_{L,SHHE}/\rho_{L0}$ is calculated by subtracting the OMR contribution, i.e., $[\Delta\rho_L(B_z) - \Delta\rho_L(B_y)]/\rho_{L0}$. Fig. 3 shows the thickness dependence of experimental $\Delta\rho_{L,SHHE}/\rho_{L0}$ at 4 T field. Meanwhile, the experimental $\Delta\rho_{T,SHHE}/\rho_{L0}$ is calculated by subtracting the linear OHE contribution from $\rho_T(B_z)/\rho_{L0}$; the result at 1 T field is displayed in Fig. 3. Fitting the thickness dependence of both longitudinal and transverse SHHE leads to $\lambda_s = 1.63 \pm 0.26$ nm. The λ_s values

are comparable to the value reported in polycrystalline Pt/sapphire at 300 K [16] and single crystalline Pt/Fe/MgO [24,25].

With the estimation of λ_s, we may fit the field dependence of SHHE signals using Eq. (1) and derive the value of θ_{SH}, τ_s, and the related diffusion coefficient $D=\lambda_s^2/\tau_s$. Fig. 4 shows fittings of both longitudinal and transverse SHHE signals from three different Pt/Al_2O_3 films. For each film, same set of parameters (θ_{SH}, λ_s, τ_s) have been used to fit both longitudinal and transverse SHHE (Sec. S4 within the Supplemental Material [21]). The derived spin transport properties of Pt are summarized in Table 1 and compared with those from Ref. [16]. One salient difference between this work and previous work [16] is that the spin relaxation time τ_s is roughly one order of magnitude longer in the epitaxial Pt films used in this work, which is critical for reaching the strong-precession condition of SHHE.

As pointed out by Dyakonov [15], for $d/\lambda_s \rightarrow 0$, the maximum longitudinal SHHE, i.e., $\Delta\rho_{L,SHHE}(\infty)/\rho_{L0}$ approaches θ_{SH}^2. As a result, $\Delta\rho_{L,SHHE}(B_z=\infty)/\rho_{L0}$ measured from thin Pt films generally provides a more precise estimation of θ_{SH}. Meanwhile, in thick Pt films, the spin precession time τ_s^* that determines the shape of the field dependence of SHHE is simply τ_s, hence measurements from thicker Pt films generally provide a more precise estimation of τ_s. Based on these arguments, we found that θ_{SH} and τ_s are most likely to be 0.022±0.006 and 1.8±0.9 ps, respectively in our Pt thin films.

The θ_{SH} value of our Pt films is lower than the values of 0.048±0.015 [24] and 0.057±0.014 [25] reported for single crystalline (001) Pt/Fe/MgO measured using spin pumping, but still lies within the range between 0.01 and 0.1 reported for polycrystalline Pt [26,27]. Crystal orientation might be responsible for the discrepancy of θ_{SH} values among different single-crystalline Pt films. It has been shown that θ_{SH} of Pt can be tuned from 1% to 10% by varying the resistivity of polycrystalline Pt films [27]. The θ_{SH} value of our Pt films is comparable to that of e-beam evaporated polycrystalline Pt films, while the longitudinal resistivity (20~50 μΩ·cm) of our Pt films at 300 K is slightly larger than that (~18 μΩ·cm) of evaporated Pt in super-clean metal regime [27]. Considering that the grain size of our (111) Pt films is small (~ 3 nm derived from x-ray diffraction), it is reasonable to postulate that abundant grain boundaries exist along charge current flow direction within Pt film plane while there are far fewer grain boundaries hindering spin current flow along the normal direction of thin film plane, which may explain the similarity of θ_{SH} values between epitaxial and polycrystalline Pt films. It is noteworthy that our epitaxial Pt films do not form interfaces with any magnetic substrates, eliminating the intricacy of separating spurious contributions, such as spin rectification effect [24,25], from ISHE contribution to the measured signals.

In conclusion, this work has demonstrated that SHHE emerges as non-linear Hall effect and non-quadratic magnetoresistance in epitaxial Pt films on Al_2O_3 substrates at room temperature. Importantly, we show that SHHE can be employed to reliably measure spin transport properties of spin-orbit coupled materials, without the complication of magnetic interfaces or the need of other measurements. The simplicity of SHHE suggests that with a magnitude up to θ_{SH}^2, they are expected to be ubiquitous in heavy metal thin film systems. Recognition of the contribution of SHHE in more complex systems (e.g., with magnetic interface) can be pivotal for understanding their entangled magnetoresistance and Hall effects.

Acknowledgment

This research was primarily supported by the U.S. Department of Energy (DOE), Office of Science, Basic Energy Sciences (BES), under Award No. DE-SC0019173. The work at NC State was supported by the U.S. Department of Energy (DOE), Office of Science, Basic Energy Sciences (BES), under Award No. DE-SC0020992. The research was performed in part in the Nebraska Nanoscale Facility: National Nanotechnology Coordinated Infrastructure and the Nebraska Center for Materials and Nanoscience (and/or NERCF), which are supported by the National Science Foundation under Award ECCS: 1542182, and the Nebraska Research Initiative.

Reference

[1] K. Y. Kato, R. C. Myers, A. C. Gossard, and D. D. Awschalom, *Observation of the Spin Hall Effect in Semiconductors*, Science **306**, 1910 (2004).

[2] J. Wunderlich, B. Kaestner, J. Sinova, and T. Jungwirth, *Experimental Observation of the Spin-Hall Effect in a Two-Dimensional Spin-Orbit Coupled Semiconductor System*, Phys. Rev. Lett. **94**, 47204 (2005).

[3] E. Saitoh, M. Ueda, H. Miyajima, and G. Tatara, *Conversion of Spin Current into Charge Current at Room Temperature: Inverse Spin-Hall Effect*, Appl. Phys. Lett. **88**, 182509 (2006).

[4] S. O. Valenzuela and M. Tinkham, *Direct Electronic Measurement of the Spin Hall Effect*, Nature **442**, 176 (2006).

[5] T. Kimura, Y. Otani, T. Sato, S. Takahashi, and S. Maekawa, *Room-Temperature Reversible Spin Hall Effect*, Phys. Rev. Lett. **98**, 156601 (2007).

[6] L. Liu, C.-F. Pai, Y. Li, H. W. Tseng, D. C. Ralph, and R. A. Buhrman, *Spin-Torque Switching with the Giant Spin Hall Effect of Tantalum*, Science **336**, 555 (2012).

[7] T. Seki, Y. Hasegawa, S. Mitani, S. Takahashi, H. Imamura, S. Maekawa, J. Nitta, and K. Takanashi, *Giant Spin Hall Effect in Perpendicularly Spin-Polarized FePt/Au Devices*, Nat. Mater. **7**, 125 (2008).

[8] H. Nakayama, M. Althammer, Y. T. Chen, K. Uchida, Y. Kajiwara, D. Kikuchi, T. Ohtani, S. Geprägs, M. Opel, S. Takahashi, R. Gross, G. E. W. Bauer, S. T. B. Goennenwein, and E. Saitoh, *Spin Hall Magnetoresistance Induced by a Nonequilibrium Proximity Effect*, Phys. Rev. Lett. **110**, 206601 (2013).

[9] Y.-T. Chen, S. Takahashi, H. Nakayama, M. Althammer, S. T. B. Goennenwein, E. Saitoh, and G. E. W. Bauer, *Theory of Spin Hall Magnetoresistance*, Phys. Rev. B **87**, 144411 (2013).

[10] Y. Cheng, S. Yu, A. S. Ahmed, M. Zhu, Y. Rao, M. Ghazisaeidi, J. Hwang, and F. Yang, *Anisotropic Magnetoresistance and Nontrivial Spin Hall Magnetoresistance in Pt/Alpha-Fe2O3 Bilayers*, Phys. Rev. B **100**, 220408 (2019).

[11] J. Fischer, O. Gomonay, R. Schlitz, K. Ganzhorn, N. Vlietstra, M. Althammer, H. Huebl, M. Opel, R. Gross, S. T. B. Goennenwein, and S. Geprägs, *Spin Hall Magnetoresistance in Antiferromagnet/Heavy-Metal Heterostructures*, Phys. Rev. B **97**, 014417 (2018).

[12] L. Baldrati, A. Ross, T. Niizeki, C. Schneider, R. Ramos, J. Cramer, O. Gomonay, M. Filianina, T. Savchenko, D. Heinze, A. Kleibert, E. Saitoh, J. Sinova, and M. Kläui, *Full Angular Dependence of the Spin Hall and Ordinary Magnetoresistance in Epitaxial Antiferromagnetic NiO(001)/Pt Thin Films*, Phys. Rev. B **98**, 024422 (2018).

[13] S. DuttaGupta, A. Kurenkov, O. A. Tretiakov, G. Krishnaswamy, G. Sala, V. Krizakova, F. Maccherozzi, S. S. Dhesi, P. Gambardella, S. Fukami, and H. Ohno, *Spin-Orbit Torque Switching of an Antiferromagnetic Metallic Heterostructure*, Nat. Commun. **11**, 5715 (2020).

[14] M. I. Dyakonov, *Spin Physics in Semiconductors* (Springer International Publishing AG,

Cham, 2017).

[15] M. I. Dyakonov, *Magnetoresistance Due to Edge Spin Accumulation*, Phys. Rev. Lett. **99**, 126601 (2007).

[16] S. Vélez, V. N. Golovach, A. Bedoya-Pinto, M. Isasa, E. Sagasta, M. Abadia, C. Rogero, L. E. Hueso, F. S. Bergeret, and F. Casanova, *Hanle Magnetoresistance in Thin Metal Films with Strong Spin-Orbit Coupling*, Phys. Rev. Lett. **116**, 16603 (2016).

[17] H. Wu, X. Zhang, C. H. Wan, B. S. Tao, L. Huang, W. J. Kong, and X. F. Han, *Hanle Magnetoresistance: The Role of Edge Spin Accumulation and Interfacial Spin Current*, Phys. Rev. B **94**, 174407 (2016).

[18] J.-C. Rojas-Sánchez, N. Reyren, P. Laczkowski, W. Savero, J.-P. Attané, C. Deranlot, M. Jamet, J.-M. George, L. Vila, and H. Jaffrès, *Spin Pumping and Inverse Spin Hall Effect in Platinum: The Essential Role of Spin-Memory Loss at Metallic Interfaces*, Phys. Rev. Lett. **112**, 106602 (2014).

[19] S. Y. Huang, X. Fan, D. Qu, Y. P. Chen, W. G. Wang, J. Wu, T. Y. Chen, J. Q. Xiao, and C. L. Chien, *Transport Magnetic Proximity Effects in Platinum*, Phys. Rev. Lett. **109**, 107204 (2012).

[20] W. Zhang, M. B. Jungfleisch, W. Jiang, Y. Liu, J. E. Pearson, S. G. E. te Velthuis, A. Hoffmann, F. Freimuth, and Y. Mokrousov, *Reduced Spin-Hall Effects from Magnetic Proximity*, Phys. Rev. B **91**, 115316 (2015).

[21] *See Supplemental Material at [URL Will Be Inserted by Publisher] for More Details on Structural Characterization, Magneto-Transport Measurements and Analysis, and the Derivation of Spin-Hall Hanle Effects.*

[22] Y. M. Lu, Y. Choi, C. M. Ortega, X. M. Cheng, J. W. Cai, S. Y. Huang, L. Sun, and C. L. Chien, *Pt Magnetic Polarization on Y3Fe5O12 and Magnetotransport Characteristics*, Phys. Rev. Lett. **110**, 147207 (2013).

[23] B. F. Miao, S. Y. Huang, D. Qu, and C. L. Chien, *Physical Origins of the New Magnetoresistance in Pt/YIG*, Phys. Rev. Lett. **112**, 236601 (2014).

[24] Y. Huo, F. L. Zeng, C. Zhou, and Y. Z. Wu, *Spin Pumping and the Inverse Spin Hall Effect in Single Crystalline Fe/Pt Heterostructure*, AIP Adv. **7**, 56024 (2017).

[25] S. Keller, L. Mihalceanu, M. R. Schweizer, P. Lang, B. Heinz, M. Geilen, T. Brächer, P. Pirro, T. Meyer, A. Conca, D. Karfaridis, G. Vourlias, T. Kehagias, B. Hillebrands, and E. T. Papaioannou, *Determination of the Spin Hall Angle in Single-Crystalline Pt Films from Spin Pumping Experiments*, New J. Phys. **20**, 53002 (2018).

[26] A. Hoffmann, *Spin Hall Effects in Metals*, IEEE Trans. Magn. **49**, 5172 (2013).

[27] E. Sagasta, Y. Omori, M. Isasa, M. Gradhand, L. E. Hueso, Y. Niimi, Y. Otani, and F. Casanova, *Tuning the Spin Hall Effect of Pt from the Moderately Dirty to the Superclean Regime*, Phys. Rev. B **94**, 60412 (2016).

Structure	**Pt thickness *d* (nm)**	**Spin Hall angle θ_{SH}**	**Spin diffusion length λ_S (nm)**	**Diffusion coefficient *D* (mm^2/s)**	**Spin relaxation time τ_S (ps)**	***T* (K)**
Pt/Al_2O_3	3.8	0.022±0.006	1.82±0.07	1.0±0.4	3.9±1.9	300
Pt/Al_2O_3	5.2	0.029±0.004	1.72±0.10	1.1±0.5	2.9±0.8	300
Pt/Al_2O_3	6.3	0.040±0.015	1.66±0.15	1.9±0.8	1.8±0.9	300
Pt/Pyrex [16]	3	0.056	0.8	3.4	0.19	100
Pt/SiO_2 [16]	3	0.056	1.4	18	0.11	100

Table 1. Comparison between spin transport properties of Pt in this work and those in reference.

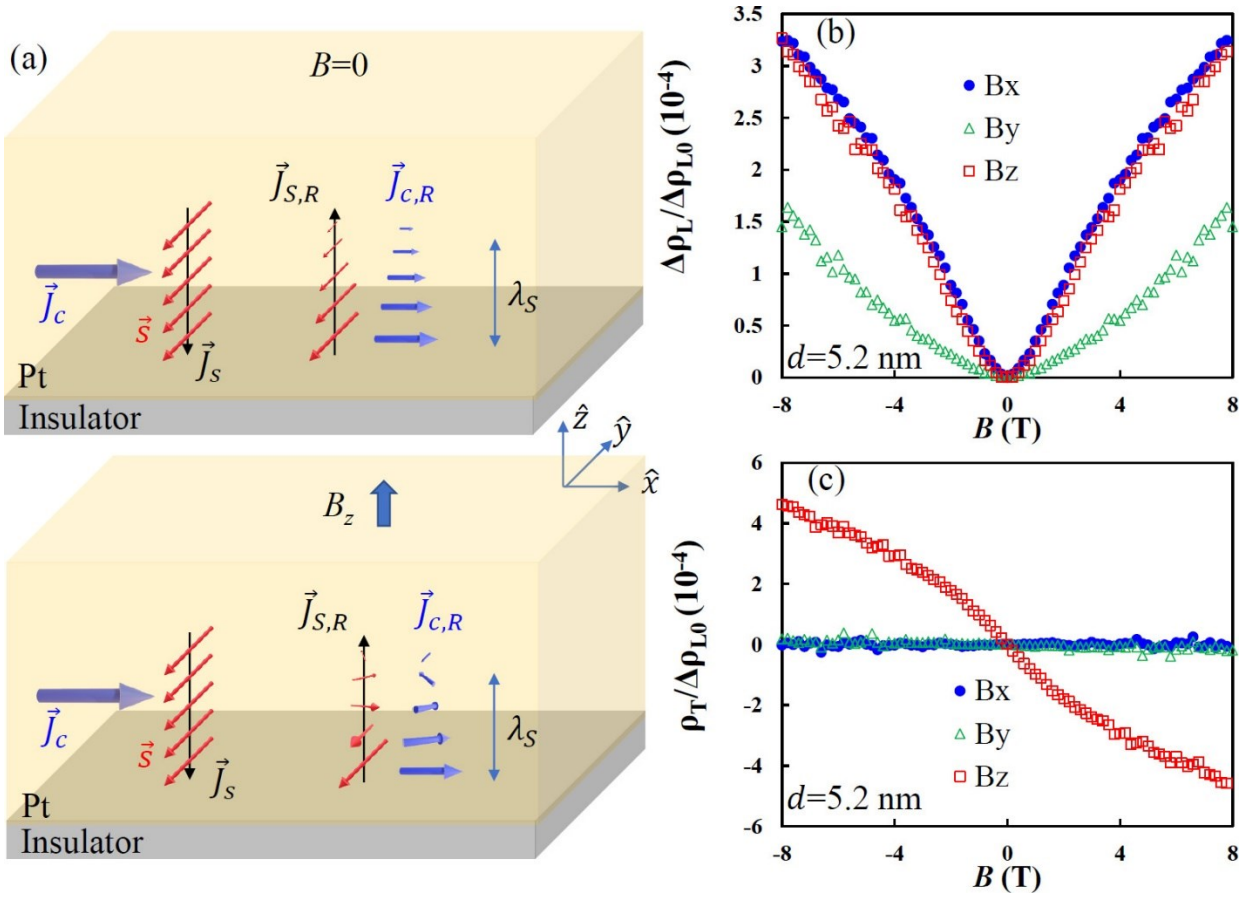

Figure 1. (a) Schematics of the spin-Hall Hanle effects at the film-substrate interface. Top: no spin precession in zero field. Bottom: spin precession when the field is perpendicular to the interface (z direction). $\vec{J}_c$ and $\vec{J}_s$ are the charge current and corresponding spin current generated via SHE respectively. $\vec{J}_{S,R}$ and $\vec{J}_{c,R}$ are the reflected spin current and the corresponding charge current generated via ISHE respectively. (b) Measured change of longitudinal resistivity normalized with the zero-field resistivity. B_x, B_y, and B_z are the magnetic field along the x, y, and z direction respectively. (c) Measured transverse Hall resistivity normalized with the zero-field longitudinal resistivity.

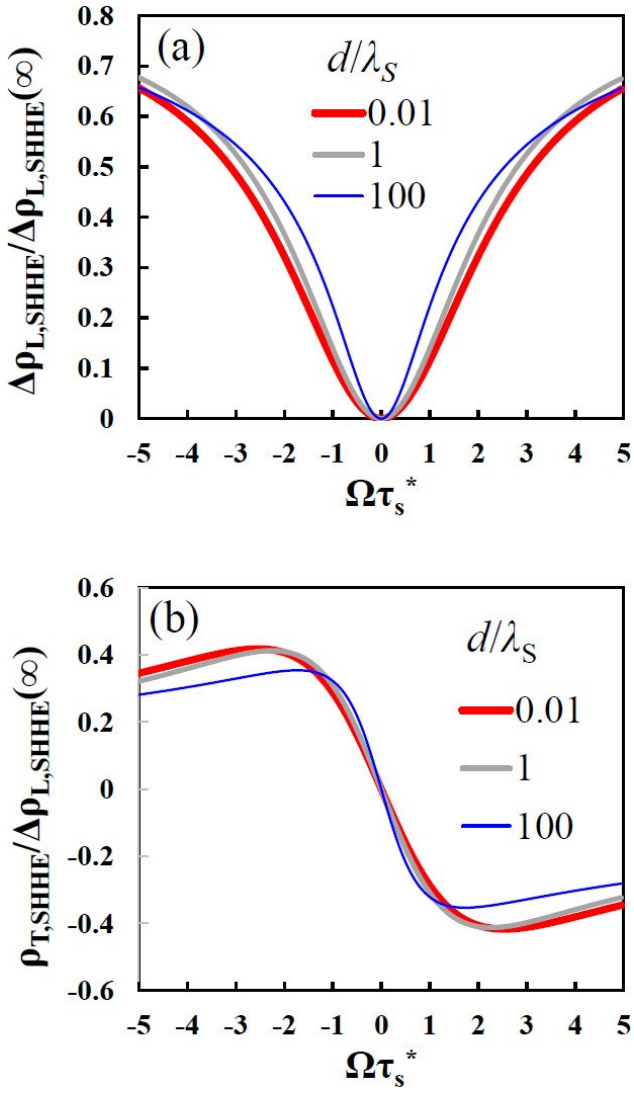

Figure 2. Simulated longitudinal (a) and transverse (b) SHHE for different d/λ_S ratio according to the real and imaginary part of Eq. (1) respectively. Both the longitudinal and the transverse effects are normalized with the maximum longitudinal SHHE which is the value at infinit field. τ_s^* is the spin precession time (see text).

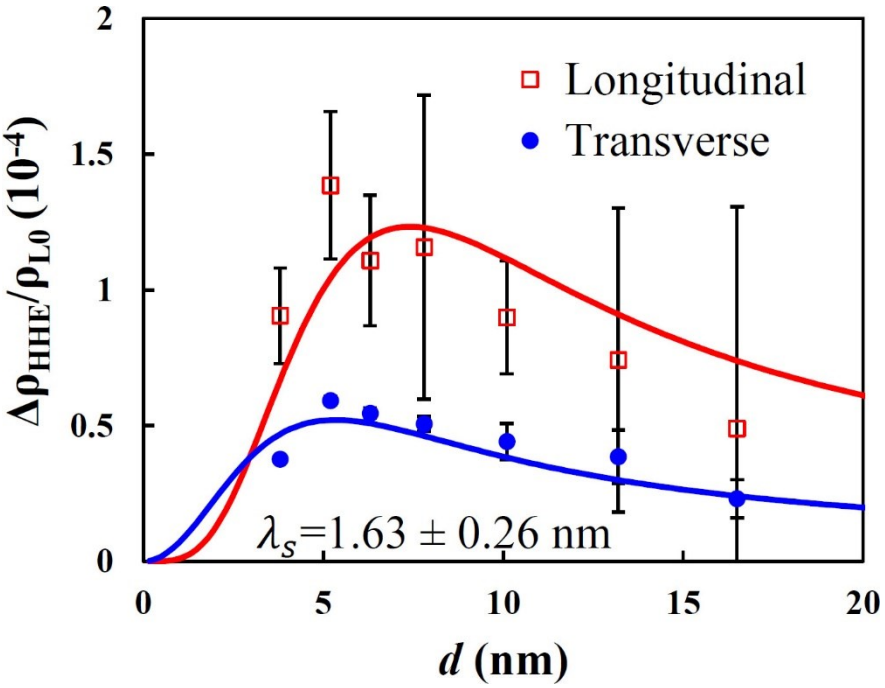

Figure 3. Longitudinal and transverse SHHE measured at 4 T and 1 T respectively, as a function of Pt thickness. The spin diffusion length estimated from the longitudinal and transverse effects are 1.63 ± 0.26 nm.

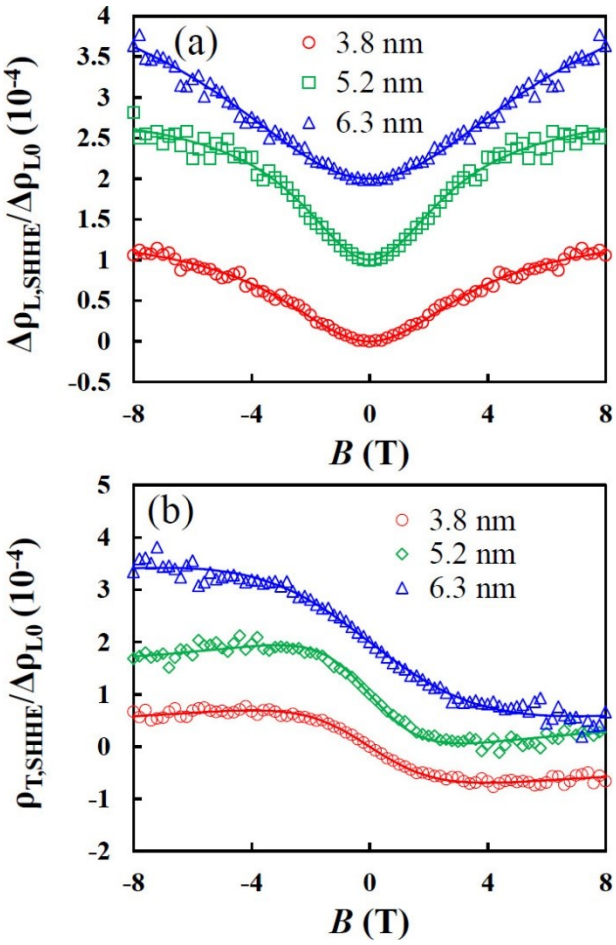

Figure 4. (a) Measured longitudinal SHHE (symbols) as the difference between the magnetoresistance in B_z and that in B_y. (b) Measured transverse SHHE (symbols) as the measured Hall effect with the linear OHE background subtracted. The data are shifted vertically in both (a) and (b) for clarity. The lines in (a) and (b) are fit of the data using Eq. (1). For each Pt film thickness, the fit uses the same set of parameters.